Supplementary materials: Observation of swallowtail catastrophe singularity in non-Hermitian bands and its topological origin

Jing Hu, Ruo-Yang Zhang, Yixiao Wang, Yifei Zhu*, Hongwei Jia†, C. T. Chan‡

1. Materials and methods

1.1 INIC for implementating non-reciprocity

To implement non-reciprocal hoppings, we use a negative impedance converter through current inversion (INIC) [1-4], as shown in Fig. S1, which incorporates a unity-gain stable operational amplifier (OpAmp) with two resisters R_a and R_b that are respectively in the positive and negative feedback circuit. When the OpAmp is operated stably in a negative feedback configuration, the input current I_1 and output current I_2 in dependence of the node voltages V_1 and V_2 can be calculated by assuming the negative potential is ideally equal to the positive input potential V_1. This yields

$$I_1 = -\frac{R_b}{R_a} \cdot i\omega C_i \cdot (V_1 - V_2) \tag{S1}$$

$$I_2 = i\omega C_i \cdot (V_1 - V_2) \tag{S2}$$

The OpAmp, being an active circuit elements, helps break the circuit reciprocity. For the experimental implementation of the anti-symmetric parts of the Hamiltonian, we require R_b=R_a, which results in

$$I_1 = -I_2 \tag{S3}$$

It can be seen that INIC makes the admittance (hopping) from the node 1 to 2 (G_{12}) and from 2 to 1(G_{21}) opposite

$$G_{12} = -i\omega C_i, G_{21} = i\omega C_i \tag{S4}$$

As viewed from node 2, it remains a positive capacitance C_i, while as seen from node 1, it acts as a negative capacitance $-C_i$.

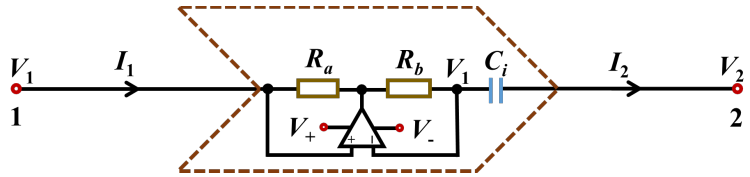

Fig.S1 Circuit diagram of a negative impedance converter structure through current inversion.

In the sample, the unity-gain stable OpAmps of model ADA4625-1ARDZ-R7 were employed. To ensure normal operations, dual supply of ±5V was provided and the frequency of the input AC current of the circuit was set as low as f = 1kHz.

1.2 Topolectric circuit design

For a grounded circuit, the Laplacian formalism for admittance matrix can be given by[4-6]

$$J = D + W - C, \tag{S5}$$

where D donates the total node conductance, W represents the ground matrix and C is the adjacency matrix. In our designed topolectric circuit with three nodes as shown in Fig. 1B, the total node conductance is a diagonal matrix

$$D = i\omega \begin{bmatrix} -C_1 - C_2 & 0 & 0 \\ 0 & C_1 + C_3 & 0 \\ 0 & 0 & C_2 + C_3 \end{bmatrix} \tag{S6}$$

Each element in the diagonal involves the conductance sum of all components connected to the corresponding node. The adjacency matrix C is characterized by

$$C = i\omega \begin{bmatrix} 0 & C_1 & C_2 \\ -C_1 & 0 & C_3 \\ -C_2 & C_3 & 0 \end{bmatrix}, \tag{S7}$$

where each element reveals the hopping achieved by capacitance between every pair of nodes. Namely, the element C_1 (C_2) represents the hopping from node b to a (c to a), while $-C_1$ ($-C_2$) is the hopping in the opposite direction—from node a to b (a to c). The two equal elements C_3 indicate that the hopping from b to c and c to b is the same. The ground matrix W reads

$$\begin{aligned} W &= i\omega \begin{bmatrix} C_g + 1/(i\omega R_g) + C_{g0} & 0 & 0 \\ 0 & C_g + 1/(i\omega R_g) & 0 \\ 0 & 0 & C_g + 1/(i\omega R_g) \end{bmatrix} \\ &= (i\omega C_g + 1/R_g) I + i\omega \begin{bmatrix} C_{g0} & 0 & 0 \\ 0 & 0 & 0 \\ 0 & 0 & 0 \end{bmatrix}, \end{aligned} \tag{S8}$$

which is also a diagonal matrix and each element denotes the contributions from grounded capacitors (C_g and C_{g0}) and resisters (R_g) to each node. Inserting these into Eq.(S5) yields

$$J = (i\omega C_g + 1/R_g) I + i\omega \begin{bmatrix} -C_1 - C_2 + C_{g0} & -C_1 & -C_2 \\ C_1 & C_1 + C_3 & -C_3 \\ C_2 & -C_3 & C_2 + C_3 \end{bmatrix} \tag{S9}$$

Compared with the Hamiltonian in Eq. (1), we set $C_1 = f_1 C_0,\ C_2 = f_2 C_0, C_3 = f_3 C_0, C_{g0} = C_0$, and finally arrive at

$$\begin{aligned} J &= \underbrace{(i\omega C_g + 1/R_g) I}_{\varepsilon_0(\omega)} + \underbrace{i\omega C_0 \begin{bmatrix} -f_1 - f_2 + 1 & -f_1 & -f_2 \\ f_1 & f_1 + f_3 & -f_3 \\ f_2 & -f_3 & f_2 + f_3 \end{bmatrix}}_{\bar{J}} \\ &= \varepsilon_0(\omega) + i\omega \bar{J} \end{aligned} \tag{S10}$$

where the effective Laplacian $\bar{J}$ is the effective Hamiltonian in Eq.(1) with a common divisor C_0 set to be 10nF, in the combined consideration of the magnitude of the Hamiltonian parameters and the

reasonable capacitance range in the circuits. The AC driving frequency of the system is an external parameter and was generally chosen as 1kHz in the experiments, leaving $\omega = 2\pi f$ constant. Therefore, the parameters f_1, f_2 and f_3 can be precisely tuned by change the coupling capacitances C_1, C_2 and C_3 respectively. The left part $\varepsilon_0(\omega)$, resulting from the equal grounded resistance $R_g = 1M\Omega$ and capacitance $C_g = 1nF$ to each node, contributes to a complex shift of the admittance eigenvalues, while leaving the admittance eigenstates invariant.

1.3 Experimental operation and observation

The experimental circuit sample is basically made up of surface mounted device (SMD) capacitors, resistors and OpAmps on a PCB. As shown in Fig1C, multiple capacitors are parallel between the three nodes as the coupling terms, and each capacitor is connected with a serial toggle switch that can be individually controlled. All the capacitances of capacitors C_1, C_2 and C_3 (with tolerance of 1%) mounted on the circuit and the corresponding f_1, f_2 and f_3 values are shown in Tab. S1. The required hooping parameters f_1, f_2 and f_3 can be realized by selecting specific C_1, C_2 and C_3 groups. Taking an exceptional points in the non-Hermitian systems, i.e. (f_1, f_2, f_3) = (0.2283, 0.1083, 0.3), as an example, it can be achieved by setting C_1=2.283nF, C_2=1.083nF and C_3 =3nF, which is a composite of the following capacitances

C_1=43pF+560pF+ 680pF+1nF;

C_2=43pF+150pF+430pF+560pF;

C_3=1.5nF+1.5nF.

To observe this point, we simply turn on the switches of the corresponding capacitors with the above values to couple the nodes, while leaving other switches off.

Tab.S1 The capacitances of C_1, C_2 and C_3 mounted on the circuit and the corresponding f_1, f_2 and f_3 values

	C_1 (Num)	f_1	C_2 (Num)	f_2	C_3 (Num)	f_3
1	43 pF (1)	0.0043	43 pF (1)	0.0043	75 pF (1)	0.0075
2	75 pF (3)	0.0075	75 pF (3)	0.0075	100 pF (3)	0.01
3	91 pF (1)	0.0091	91 pF (1)	0.0091	150 pF (1)	0.015
4	100 pF (3)	0.01	100 pF (3)	0.01	300 pF (3)	0.03
5	150 pF (4)	0.015	150 pF (4)	0.015	1 nF (2)	0.1
6	300 pF (7)	0.03	300 pF (7)	0.03	1.5 nF (3)	0.15
7	430 pF (1)	0.043	430 pF (1)	0.043		
8	470 pF (1)	0.047	470 pF (1)	0.047		
9	560 pF (1)	0.056	560 pF (1)	0.056		
10	680 pF (2)	0.068	680 pF (2)	0.068		
11	750 pF (1)	0.075	750 pF (1)	0.075		
12	820 pF (3)	0.082	820 pF (3)	0.082		
13	910 pF (1)	0.091	910 pF (1)	0.091		
14	1 nF (5)	0.1	1 nF (5)	0.1		
15	1.2 nF (2)	0.12	1.2 nF (2)	0.12		

16	1.5 nF (1)	0.15	1.5 nF (1)	0.15		
17	1.8 nF (1)	0.18	1.8 nF (1)	0.18		

In the experiments, a DC power supply (GPC-3030) served as the dual voltages of ±5V for the OpAmps to operate normally. A waveform generator (Keysight: M3201A) was used to excite the system and a sinusoidal voltage with constant amplitude (generally 1V~2V) and frequency of 1khz was set to feed into each node of the circuit individually, while a matching oscilloscope (RS PRO IDS1074B) was employed to measure the voltage response of all nodes in the system. The input current can be acquired by connecting a shunt resistor of R=10 Ω from the input node to the voltage source.

From the measured voltage response to the input current vector, one can directly obtain the Green's function matrix G, which is inverse of admittance matrix J [1-8]. The admittance eigenvalues and eigenstates are thus easily retrieved from the Green's function G.

2. Riemannian geometry

Here we demonstrate that the adiabatic transformation process of eigenstates within energy gaps is Riemannian geometry. The metric operator in pseudo-Hermiticity plays a similar role to the space-time metric in general relativity [9]. The time varying problem is governed by

$$H\left|\varphi_m\right\rangle = i\partial_t\left|\varphi_m\right\rangle \tag{S11}$$

and the completeness of eigenstates shows that a field can be expanded as

$$\phi_n(\lambda(t)) = \sum_m [U(\lambda(t))]^{-1}{}_n{}^m \varphi_m(\lambda(t)) \tag{S12}$$

Applying the partial derivative with respect to t, one obtains

$$\begin{aligned} i\frac{\partial}{\partial t}\phi_n(\lambda(t)) &= H[U(\lambda(t))]^{-1}{}_n{}^m \varphi_m(\lambda(t)) \\ &= i\frac{\partial[U(\lambda(t))]^{-1}{}_n{}^m}{\partial t}\varphi_m(\lambda(t)) + i[U(\lambda(t))]^{-1}{}_n{}^m \frac{\partial\varphi_m(\lambda(t))}{\partial t} \end{aligned} \tag{S13}$$

The adiabatic approximation allows the instantaneous eigenvalue problem

$$H(\lambda(t))\varphi_m(\lambda(t)) = E_m\varphi_m(\lambda(t)) \tag{S14}$$

and applying a scalar product $\left\langle\varphi_l\right|$ from the left of Eq. S13 yields

$$-iE_l[U(\lambda(t))]^{-1}{}_n{}^l = \frac{\partial[U(\lambda(t))]^{-1}{}_n{}^l}{\partial t} + \left\langle\varphi_l\right|\eta\frac{\partial\left|\varphi_m(\lambda(t))\right\rangle}{\partial t}[U(\lambda(t))]^{-1}{}_n{}^m \tag{S15}$$

The partial derivative with respect to t can be expanded as

$$\frac{\partial\left|\varphi_m(\lambda(t))\right\rangle}{\partial t} = \sum_k \frac{\partial\left|\varphi_m(\lambda(t))\right\rangle}{\partial\lambda^k}\frac{\partial\lambda^k}{\partial t} \tag{S16}$$

We define the affine connection

$$A_k{}^n{}_m = -\langle \varphi_n | \eta \frac{\partial | \varphi_m(\lambda(t)) \rangle}{\partial \lambda^k} = -\langle \varphi_n | \eta \frac{\partial}{\partial \lambda^k} | \varphi_m \rangle \tag{S17}$$

and the solution for U^{-1} is thus obtained as

$$U^{-1} = \exp[\int_0^t ds \frac{\partial \lambda^k}{\partial s} A_k - i\int_0^t ds\omega(\lambda(s))] = \exp(\int_{\lambda(0)}^{\lambda(t)} d\lambda^k A_k) \times \exp[i\int_0^t dsE(\lambda(s))] \tag{S18}$$

Ignoring the dynamical phase, the geometric phase is simply

$$U^{-1} = \mathrm{P}\exp(\int_{\lambda(0)}^{\lambda(t)} d\lambda^k A_k) \tag{S19}$$

where P denotes path ordering operator. It is important to add the path ordering operator here, because the affine connection A is a matrix. Hence, A is a non-Abelian parallel transport gauge [10], and the integration of A on closed loops depends on the path. Here we define a local metric g with its elements being

$$g_{mn} = \langle \varphi_m | \eta \varphi_n \rangle \tag{S20}$$

which has explicit relations with the affine connection. The normalization of eigenstates can make g a constant and hence the partial derivative with respect to time vanishes

$$0 = \partial_t g_{mn} = \partial_t \langle \varphi_m | \eta \varphi_n \rangle \tag{S21}$$

Inserting the identity operator $I = \sum_l \eta | \varphi_l \rangle \langle \varphi_l |$, one obtains

$$\partial_{\lambda_k} \langle \varphi_m | \eta \varphi_n \rangle = \sum_l \langle \partial_{\lambda_k} \varphi_m | \eta | \varphi_l \rangle \langle \varphi_l | \eta \varphi_n \rangle + \sum_l \langle \varphi_m | \eta | \varphi_l \rangle \langle \varphi_l | \eta \partial_{\lambda_k} \varphi_n \rangle \tag{S21}$$

We note that

$$\langle \partial_{\lambda_k} \varphi_m | \eta | \varphi_l \rangle = \langle \varphi_l | \eta | \partial_{\lambda_k} \varphi_m \rangle^* \tag{S22}$$

and hence we have

$$0 = A_k^{*l}{}_m g_{ln} + g_{ml} A_k{}^l{}_n \tag{S23}$$

This equation is an important relation between the metric g and the affine connection, revealing the Riemannian geometry of the adiabatic transformation process. In the next section, we will use this equation to predict the emergence of exceptional surfaces (ESs) and nodal lines.

3. The emergence of ESs in view of Riemannian geometry

The metric operator in determining the pseudo-Hermitian symmetry of the considered system is the Riemannian metric. In real line gaps, there are three real eigenstates, due to the fact that the system preserves PT symmetry and the Hamiltonian has been gauged to be real. These eigenstates are orthogonal under an indefinite inner product

$$\langle \varphi_m | \eta \varphi_n \rangle \begin{cases} = 0 & m \neq n \\ \neq 0 & m = n \end{cases} \tag{S24}$$

and thus the metric g is diagonal and real. Within the three diagonal elements in g, two of which are positive, and the other is negative, i.e. the following three forms

$$g_1=\begin{bmatrix}-1&0&0\\0&1&0\\0&0&1\end{bmatrix},\ g_2=\begin{bmatrix}1&0&0\\0&-1&0\\0&0&1\end{bmatrix},\ g_3=\begin{bmatrix}1&0&0\\0&1&0\\0&0&-1\end{bmatrix} \tag{S24}$$

In the swallowtail catastrophe, the parameter space is partitioned into several regions by the ESs, as shown in Fig. S2A. Here Regs I and II are *PT* exact phases, and Reg III is *PT* broken phase.

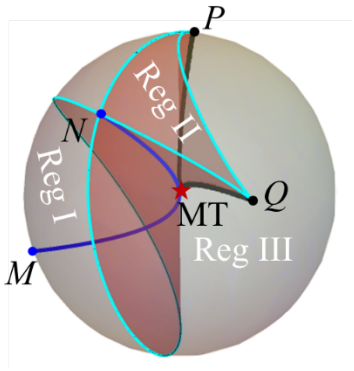

Fig. S2. Different regions partitioned by ESs. Regs I and II: PT exact phases. Reg III: PT broken phase.

We take Reg I as an example to show that the Riemannian geometry can be used to predict the emergence of ES and nodal line. The local metric of Reg I is g_1. Since the eigenstates are real, the definition (Eq. S17) shows that the affine connection is also real. Hence, Eq. 13 reduces to

$$0=A_k{}^l{}_m g_{ln}+g_{ml}A_k{}^l{}_n \tag{S25}$$

The metric is diagonal, and one can easily demonstrate that the connection is a linear combination of the following elementary matrices

$$T_1=\begin{bmatrix}0&1&0\\1&0&0\\0&0&0\end{bmatrix},\ T_2=\begin{bmatrix}0&0&1\\0&0&0\\1&0&0\end{bmatrix},\ T_3=\begin{bmatrix}0&0&0\\0&0&-1\\0&1&0\end{bmatrix} \tag{S26}$$

which are exactly the Lie algebraic generators of SO(2,1) group. It is shown that T_1 and T_2 characterize Lorentz boost of φ_1 and φ_2, and φ_1 and φ_3, respectively. T_3 characterizes the rotation of φ_2 and φ_3. The π rotation of φ_2 and φ_3

$$[\varphi_1,\varphi_2,\varphi_3]\exp(\pi T_3)=[\varphi_1,-\varphi_2,-\varphi_3] \tag{S27}$$

brings them to their opposite directions, which are still the eigenstate at the same point in parameter space. Consider the eigenstates adiabatically evolve on a closed loop, and accumulate a π geometric phase as Eq. S27. The loop simply circulates the nodal line (NL), and the polarizations of φ_1 and φ_2 rotate π as indicated by Fig. 2C2, due to the matrix form geometric phase πT_3. This is a way for predicting the existence of the NL formed by the first and the second bands. The ES can also be predicted. The Lorentz transformation between the first and the second bands can be characterized by

$$[\varphi_1, \varphi_2, \varphi_3]\exp(\beta T_1) \tag{S28}$$

and the matrix exponential is

$$\exp(\beta T_1) = \begin{bmatrix} \cosh\beta & \sinh\beta & 0 \\ \sinh\beta & \cosh\beta & 0 \\ 0 & 0 & 1 \end{bmatrix} \tag{S29}$$

As β approaches +∞, we have the relation $\cosh\beta \approx \sinh\beta = \rho$, resulting in two parallel vectors in the same directions

$$\begin{aligned} \varphi_1 \cosh\beta + \varphi_2 \sinh\beta &= \rho(\varphi_1 + \varphi_2) \\ \varphi_1 \sinh\beta + \varphi_2 \cosh\beta &= \rho(\varphi_1 + \varphi_2) \end{aligned} \tag{S30}$$

Similarly, as β approaches –∞, $\cosh\beta \approx -\sinh\beta = \rho$, resulting in another pair of parallel vectors in opposite directions

$$\begin{aligned} \varphi_1 \cosh\beta + \varphi_2 \sinh\beta &= \rho(\varphi_1 - \varphi_2) \\ \varphi_1 \sinh\beta + \varphi_2 \cosh\beta &= -\rho(\varphi_1 - \varphi_2) \end{aligned} \tag{S31}$$

In band gaps, β cannot approach infinity by an integration on a path, and an infinitely large β can only be provided by approaching the exceptional surfaces. The eigenstates that coalesce are φ_1 and φ_2, and thus the ES, being the boundary of Reg I, can be formed by the second and third bands. We note that the φ_1 and φ_3 also experience Lorentz boost, but the second band blocks the formation of ES between the first and the third bands. However, if we consider Reg III with metric g_2, the generators will be

$$T_1' = \begin{bmatrix} 0 & 1 & 0 \\ 1 & 0 & 0 \\ 0 & 0 & 0 \end{bmatrix},\ T_2' = \begin{bmatrix} 0 & 0 & -1 \\ 0 & 0 & 0 \\ 1 & 0 & 0 \end{bmatrix},\ T_3' = \begin{bmatrix} 0 & 0 & 0 \\ 0 & 0 & 1 \\ 0 & 1 & 0 \end{bmatrix} \tag{S32}$$

meaning that ESs can be formed by the first and the second bands, or by the second and the third bands (due to Lorentz boost characterized by T_1 and T_3). We also note that there is another rotation of φ_1 and φ_3 (i.e. $\exp(\pi T'_2)$), but the second band blocks the formation of NL by the first and the third bands. Regions having the local metric g_3 is also possible, and in the considered parameter ranges of the Hamiltonian (Eq. 1 in the maintext), such regions are not present. We will not give more analysis. It is notable that for real line gaps, regions with different metrics are not connected, and they are separated by imaginary line gaps.

The imaginary line gaps have very different forms of metrics compared with the real line gaps. In broken phases, there will always be a pair of eigenstates that are conjugate to each other, and the other eigenstate is real. The local metric in broken phase is not diagonal, but is a Hermitian matrix instead. Possible forms can be

$$g_4 = \begin{bmatrix} 0 & 1 & 0 \\ 1 & 0 & 0 \\ 0 & 0 & 1 \end{bmatrix},\ g_5 = \begin{bmatrix} 1 & 0 & 0 \\ 0 & 0 & 1 \\ 0 & 1 & 0 \end{bmatrix} \tag{S33}$$

The regions with different metrics in broken phase are path connected, contrary to exact phases. The boundary between regions with different metrics is a surface with real parts of all three eigenvalues being degenerate. The surface is not exactly a degeneracy because the imaginary parts of eigenvalues are not degenerate.

4. ADE classification of swallowtail: A4 singularity (To be supplemented)

Before introducing ADE classification, we firstly need to introduce another mathematical concept, which is the orbifold. An orbifold is much like a smooth manifold but possibly with singularities of the form of fixed points of finite group actions. A smooth manifold is a space locally modelled on Cartesian space/Euclidean spaces $\mathbf{R}^n$, an orbifold is, more generally, a space that is locally modelled on smooth action groupoids (homotopy quotients) $\mathbf{R}^n//G$ of a finite group G on a Cartesian space.

An n-dimensional orbifold is a Hausdorff topological space X, called the underlying space, with a covering by a collection of open subsets U_i, closed under finite intersections. For each U_i, there is:

1. an open subset V_i of $\mathbf{R}^n$, invariant under a faithful linear action of finite group Γ_i;
2. a continuous map φ_i of V_i onto U_i invariant under Γ_i, called an orbifold chart, which defines a homeomorphism between V_i/Γ_i, and U_i.

The collection of orbifold charts is called an orbifold atlas if the following properties are satisfied:

1. for each inclusion $U_i \subset U_j$ there is an injective group homeomorphism f_{ij}: $\Gamma_i \to \Gamma_j$
2. for each inclusion $U_i \subset U_j$ there is a Γ_i-equivalent homeomorphism ψ_{ij}, called a gluing map, of V_i onto an open subset of V_i
3. the gluing maps are compatible with the charts, i.e. $\varphi_j\psi_{ij}=\varphi_i$
4. the gluing maps are unique up to composition with group elements, i.e. any other possible gluing map from V_i to V_j has the form $g.\psi_{ij}$ for a unique g in Γ_j

The orbifold atlas defines the orbifold structure completely: two orbifold atlases of X give the same orbifold structure if they can be consistently combined to give a larger orbifold atlas. Note that the orbifold structure determines the isotropy of any point of the orbifold up to isomorphism: it can be computed as the stabilizer of the point in any orbifold chart. If $U_i \subset U_j \subset U_k$, then there is a unique transition element g_{ijk} in Γ_k such that $g_{ijk}\psi_{ik}=\psi_{jk}\psi_{ij}$. These transition elements satisfy $(\mathrm{Ad}g_{ijk}).f_{ik}=f_{jk}.f_{ij}$, as well as the cocycle relation $f_{km}.(g_{ijk}).g_{ikm}=g_{ijm}.g_{jkm}$.

In mathematics, the ADE classification (originally A-D-E classifications) is a situation where certain kinds of objects are in correspondence with simply laced Dynkin diagrams. The complete list of simply laced Dynkin diagrams comprises

$$A_n,\ D_n,\ E_6,\ E_7,\ E_8. \tag{S34}$$

Here "simply laced" means that there are no multiple edges, which corresponds to all simple roots in the root system forming angles of $\pi/2=90°$ (no edge between the vertices) or $2\pi/3=120°$ (single edge between the vertices). These are two of the four families of Dynkin diagrams (omitting B_n and C_n), and three of the five exceptional Dynkin diagrams (omitting F_4 and G_2).

In terms of *compact Lie algebras* and corresponding simply laced Lie groups:

- A_n corresponds to ⑩❶$_{n+1}$, the algebra of the special unitary group $SU(n+1)$;
- D_n corresponds to ⑩⑥$_{2n}$, the algebra of the even projective special orthogonal group $PSO(2n)$, while
- E_6, E_7, E_8 are three of five exceptional compact Lie algebras.

An ADE singularity is an orbifold fixed point locally of the form $\mathbf{C}^n//\Gamma$ with $\Gamma \hookrightarrow SU(2)$ a finite subgroup of $SU(2)$ given by the ADE classification (and $SU(2)$ is understood with its defining linear action on the complex vector space $\mathbf{C}^2$).

5. Loops, hypersurface singularities, and fractional topological invariants

In non-Hermitian systems, it is possible that a topological invariant is not an integer, but a fraction instead. In this section, we will discuss some possible singularities that carry fractional invariants. Complete intersections (NILs), cusps (EL3s) will be included in the discussion.

Before discussing the fractional invariant, we should provide the definition of fractional topology. In topological physics, adding a minus sigh to a state is treaded to be the same state. Hence, if eigenstates of a Hamiltonian evolve to its negative $\varphi \to -\varphi$ via adiabatic transformation on a closed loop, the eigenstates are considered to have evolved to the initial states. Such a loop carries an integer topological invariant, and representative examples are loops circulating 2D Dirac points [12] or 3D nodal lines [13] in Hermitian systems. However, multiplying the state by an imaginary unit is not regarded as the same state, and thus the loops bringing φ to $i\varphi$ is not considered to have evolved to the initial state. Such loops carry fractional topological invariants. To obtain an integer invariant, more cycles of adiabatic transformation on the loop is required. In some cases, one eigenstate can evolve to another eigenstate on a closed loop, which is also a representative example. Next, we will discuss these situations in detail.

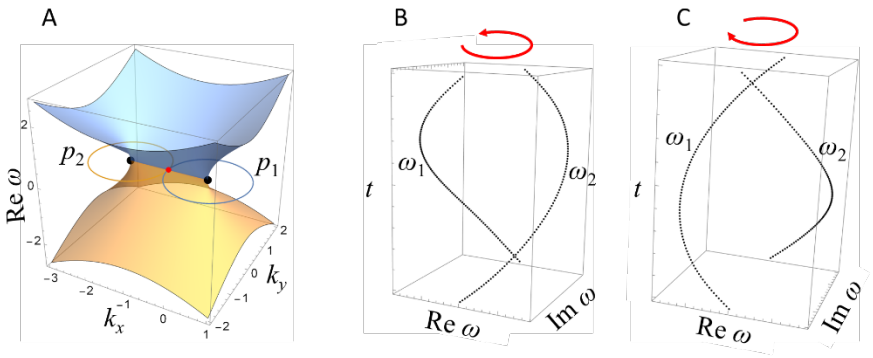

Fig. S3. Fractional winding number of isolated exceptional point induced by band braiding.

Firstly, let us consider a simple example, which is a two-band model and the Hamiltonian takes the form

$$H(\mathbf{k}) = (\sigma_1 + i\sigma_2) + k_x\sigma_1 + k_y\sigma_2 \tag{S34}$$

The band structure is shown in Fig. S3A, which has two isolated exceptional points (EPs) in parameter space. It can be easily found that the two EPs comes from the splitting of a Hermitian Dirac point by introducing non-Hermitian perturbations (the term $i\sigma_2$ in Eq. S34). The topology of the two EPs can be investigated by closed loops p_1 and p_2 circulating them (p_1 and p_2 have the same basepoint, the red point in Fig. S3A). By observing the evolution of eigenvalues on a closed loop circulating the EP, the two

eigenvalues braid, resulting an exchange $\omega_1 \leftrightarrow \omega_2$ (simultaneously $\varphi_1 \leftrightarrow \varphi_2$, see Fig. S3B-C). It is obvious that the eigenstates cannot evolve to the initial states after one cycle on the loops, and the topological invariant carried by the loop is a fraction. However, if one consider the composite loop p_1p_2, the braiding of the eigenvalues will cancel, because the eigenvalues are braiding in opposite directions (see the red arrows in Fig. S3B-C). The composite loop carries an integer topological invariant, on which the eigenstates will accumulate a π geometric phase, equivalent to the topology a 2D Dirac point. Two cycles on the loop (p_1 or p_2) will result in the braiding of eigenvalues twice ($\omega_1 \to \omega_2 \to \omega_1$, $\omega_2 \to \omega_1 \to \omega_2$), and eigenstates can evolve to their negatives ($\varphi_1 \to -\varphi_1$, $\varphi_2 \to -\varphi_2$), accumulating π geometric phase. Hence, the winding number of the exceptional point is a half integer (i.e. 1/2). It is notable that the integration of Berry connection on one cycle of the loop is not gauge independent, due to the fact that the eigenstates cannot evolve to the initial states. To avoid such problems, some researchers would like to use energy vorticity to define a gauge independent topological invariant [11]. If one would like to employ the adiabatic transformation of eigenstates, the geometric phase will be accumulated on n cycles on the closed loops [13], so that the eigenstates can evolve to the initial states to ensure gauge independence. If the total geometric phase is $m\pi$, the topological invariant is simply the fraction m/n.

Next, we consider the complete intersections and cusps in our Hamiltonian. The NIL is an intersection of ESs, and the corresponding Hamiltonian is a non-defective matrix and can be diagonalized. While the Hamiltonian on ES is defective (lacking one eigenstate) and cannot be diagonalized. It can be easily identified that the eigenstates at the NIL come from the contributions of the intersecting ESs. The topology of such singularities are characterized by the loops l_2 and l_7 in Fig. 2A and Fig. 3A in the maintext [15], whose base points are on NIL. In view of the adiabatic transformations, the eigenstates on one ES evolve to the eigenstates on the other ES. *An equivalent statement is that one eigenstate of the NIL adiabatically evolves to the other eigenstate of the NIL*. It is obvious that such process cannot bring the eigenstates to the initial states, and thus carry fractional topological invariants. To obtain a gauge independent topological invariant, we need to consider the loops l_2^2 and l_7^2 in Fig. 2A and Fig. 3A in the maintext. Since eigenstates φ_2 and φ_3 rotate $\mp\pi$ ($\varphi_{2,3} \to -\varphi_{2,3}$, see Fig. 2D and Fig. 3E in the maintext), the eigenstates evolve to the initial state, which carry integer topological invariants. Correspondingly, the winding numbers on l_2 and l_7 are both half integers (i.e. 1/2).

The EL3s are a little different from the NIL. In catastrophe theory, the cusps are formed due to the folding of curves in higher dimensions [16]. In band structures, the EL3s are formed in the same way. As can be obviously indicated from Fig. 2-3 in the maintext that the ES is folded at the cusps. Hence, on loop l_3 (Fig. 2A), the eigenvalues experience order exchange twice ($\omega_1 \to \omega_{2,3} \to \omega_1$ and $\omega_{2,3} \to \omega_1 \to \omega_{2,3}$) at each of the cusps, due to the folding of ES. The eigenstates $\varphi_1 \sim \varphi_3$ experience ($-\pi$, 0, π) rotations on the loop, meaning that the eigenstates return to the initial states, and thus l_3 carries an integer topological invariant. However, the loop l_3 can be decomposed into two sub-loops l_8 and l_9 (see Fig. S4A), and each loop circulates one EL3. The eigenvalues on the sub-loop l_8 will experience order exchange once, and thus the final states on the loop are different from the initial states (see Fig. S4B). One may consider if the cusp is similar to the complete intersection, carrying a half integer winding number. In fact, the current case is a little different, because in cusps, all three eigenstates are involved (the NIL only involves two eigenstates). As shown in Fig. S4B-C, the eigenvalues experience the following processes of order change on l_8: starting from the ES, in the first cycle, band 2 and band 3 bifurcate in the gap, and then band 1 and band 2 coalesce on the other ES. After the parameters traverse the EL3, the coalesced bands (1 and 2) exchange the order with band 3, and finally the band sequence is rearranged as (2,3,1). Such process will be repeated on the second and third cycles, and the

sequences are rearranged as (3,1,2) and (1,2,3). Next, we turn our attention to the eigenstates. The adiabatic transformation process of eigenstates on loops l_8 of three cycles is shown in Fig. S4D. The eigenstates evolve to the initial states, and the accumulated geometric phase can be obtained as 2π. Hence, the winding number on l_8 (also l_9) is 2/3 instead of 1/2. Now we consider the loop l_4, which encloses the double EL3s in the broken phase region (see Fig. 3A in the maintext). Similar to l_3, l_4 also traverses the cusps twice, leading to the order exchange of eigenvalues simultaneously. However, in broken phase regions, there exist a surface, on which the real part of all three eigenvalues are degenerate (we call it quasi-degeneracy), and if the loop l_4 traverses surface (at least twice, or multiples of two times), the eigenvalues will also experience order exchange twice. Hence, the decomposed sub-loops l_{10} and l_{11} of l_4 (see Fig. S4), will be very different from l_8 and l_9. Let us take l_{10} as an example, the loop traverses the quasi-degeneracy and EL3, experiencing the order exchange process of eigenvalues $\omega_{2,3} \to \omega_1 \to \omega_{2,3}$. As for eigenstates, φ_2 and φ_3 rotate $\pm\pi/2$ for one cycle on the loop, meaning that the eigenstates cannot evolve to the initial states (see Fig. S3). The eigenstates can evolve to the initial states for two cycles, bringing φ_2 and φ_3 to the their negatives (i.e. $\pm\pi$ for φ_2 and φ_3). This adiabatic transformation process shows that l_{10} and l_{11} both carry half integer (i.e. 1/2) winding numbers.

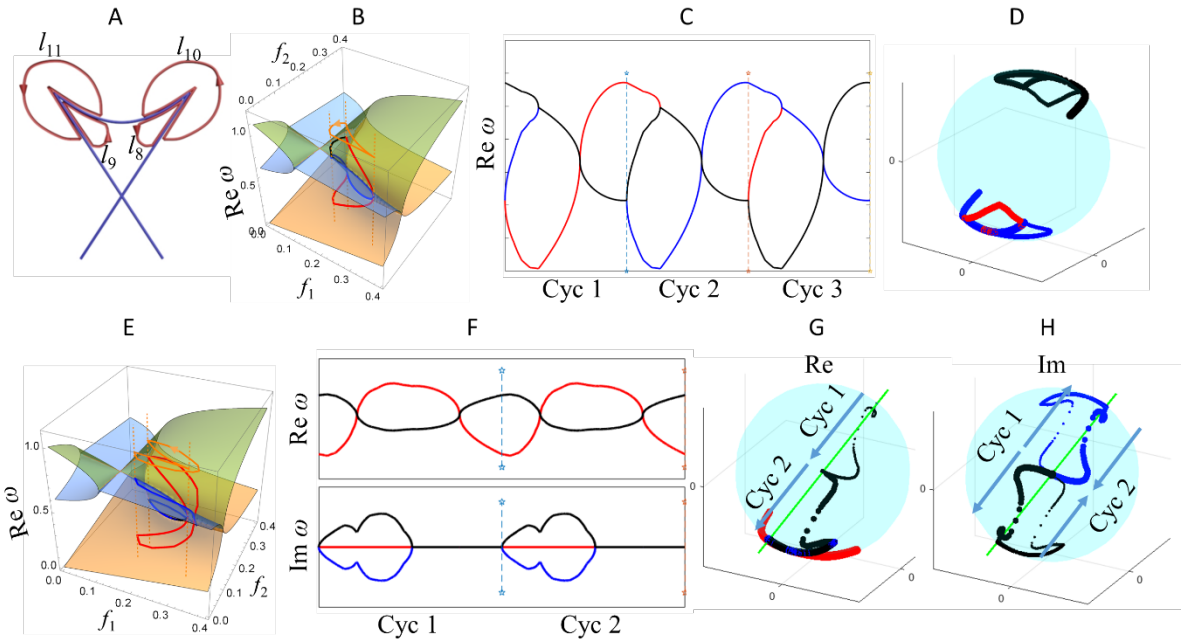

Fig. S4. Band folding induced fractional winding number at EL3s. A. sub-loops enclosing EL3s in exact phases (l_8 and l_9) and broken phases (l_{10} and l_{11}). B. Eigenvalues at loop l_8, band 2 (blue, the corresponding eigenstate φ_2) and band 3 (black, the corresponding eigenstate φ_3) coalesce at ES, and exchange order with band 1 (red, the corresponding eigenstate φ_1) at EL3. C. Evolution of eigenvalues on loop l_8 for three cycles. D. Adiabatic transformation of eigenstates on l_8 for three cycles (red, φ_1; blue, φ_2; black, φ_3). E. Eigenvalues at loop l_{10}. F. Evolution of eigenvalues on loop l_{10} for two cycles. G-H. Adiabatic transformation of eigenstates on l_8 for two cycles. G. real parts of eigenstates. H. Imaginary parts of eigenstates.

The above discussions provides a conclusion that singularities with fractional topological are often present in pairs, because it is always obtained from a splitting of a singularity carrying integer topological invariant. On a closed loop circulating a singularity with an integer topological invariant, both the eigenvalues and eigenstates can evolve to the initial state, which is totally opposite to the

singularity with fractional invariant. The non-Hermiticity introduces a degree of freedom that eigenvalues can exchange orders (braiding or band fold) or coalesce (exceptional surface), which can break a loop (with integer invariant) into two sub-loops (with fractional invariants). This is the intrinsic factor for obtaining a singularity with fractional topological invariant.

6. Sequence of eigenstates and hybrid topological invariant

Intersection singularities have hybrid topological invariants. In [14], the hybrid invariant is illustrated by extending the parameters into complex space. However, in the considered system, extending the parameters into complex space will break the *PT* symmetry and η-pseudo-Hermitian symmetry. The swallowtail catastrophe is not expected to emerge if the symmetries are broken. Actually, in the original parameter space (parameters being real) without extending the dimensions, the hybrid invariant nature can also be illustrated [15]. Next, we will discuss the impact of the sequence of two eigenstates forming ES on the topological invariants carried by these loops. This is the intrinsic property in determining the nature of hybrid topological invariant of hypersurface singularities.

Tab.S2. Hybrid invariant on the closed loop circulating NIL

$\alpha_2\alpha_7\alpha_2\alpha_7$	$\alpha_2\alpha_7\alpha_2\alpha_7^{-1}$	$\alpha_2^{-1}\alpha_7^{-1}\alpha_2^{-1}\alpha_7$	$\alpha_2^{-1}\alpha_7^{-1}\alpha_2^{-1}\alpha_7^{-1}$
$\alpha_2\alpha_7\alpha_2^{-1}\alpha_7^{-1}$	$\alpha_2\alpha_7^{-1}\alpha_2^{-1}\alpha_7$	$\alpha_2^{-1}\alpha_7\alpha_2\alpha_7^{-1}$	$\alpha_2^{-1}\alpha_7^{-1}\alpha_2\alpha_7$
$\alpha_2^{-1}\alpha_7\alpha_2^{-1}\alpha_7$	$\alpha_2\alpha_7^{-1}\alpha_2^{-1}\alpha_7^{-1}$	$\alpha_2^{-1}\alpha_7\alpha_2\alpha_7$	$\alpha_2\alpha_7^{-1}\alpha_2\alpha_7^{-1}$
$\alpha_2^{-1}\alpha_7\alpha_2^{-1}\alpha_7^{-1}$	$\alpha_2^{-1}\alpha_7^{-1}\alpha_2\alpha_7^{-1}$	$\alpha_2\alpha_7\alpha_2^{-1}\alpha_7$	$\alpha_2\alpha_7^{-1}\alpha_2\alpha_7$

Tab.S3. Hybrid invariant on the closed loop circulating EL3

$\alpha_{10}\alpha_8$	$\alpha_{10}\alpha_8^{-1}$
$\alpha_{10}^{-1}\alpha_8$	$\alpha_{10}^{-1}\alpha_8^{-1}$

For an isolated singularity, a common approach in characterizing the topology is simply observing the adiabatic transformation process on a closed loop circulating it. However, if one considers a hypersurface singularity, the situation will be a little different. For example, a closed loop circulating the intersection NIL will inevitably be decomposed into a composite of four elementary loops (see Fig. S4). In the maintext, we have shown that on loops l_2 and l_7, the eigenstates will bifurcate and rotate in opposite directions as the parameters depart from ES, which shows that if the order of φ_2 and φ_3, one simply obtains the inverse of the topological invariant on the loops [15]. Now we denote α_2 and α_7 as the topological invariants on loops l_2 and l_7, respectively. If a loop traverses an ES, the sequence of the two eigenstates forming the ES will have two different options. Hence, for a loop circulating the NIL, there will be 2^4=16 invariants (as listed in Table S2). All the 16 invariants are integers because eigenstates evolve to the initial states. The loop circulating an EL3 will is composite of l_{10} and l_8 (with invariants α_{10} and α_8) and thus have 2^2=4 invariants, as listed in Table S3. Different from the NIL, the invariants on such loops circulating an EL3 are all fractions. The adiabatic transformation of eigenstates for two invariants $\alpha_{10}\alpha_8$ and $\alpha_{10}\alpha_8^{-1}$ are shown in Fig. S5, showing that the winding numbers are 2/3 and 1/2, respectively.

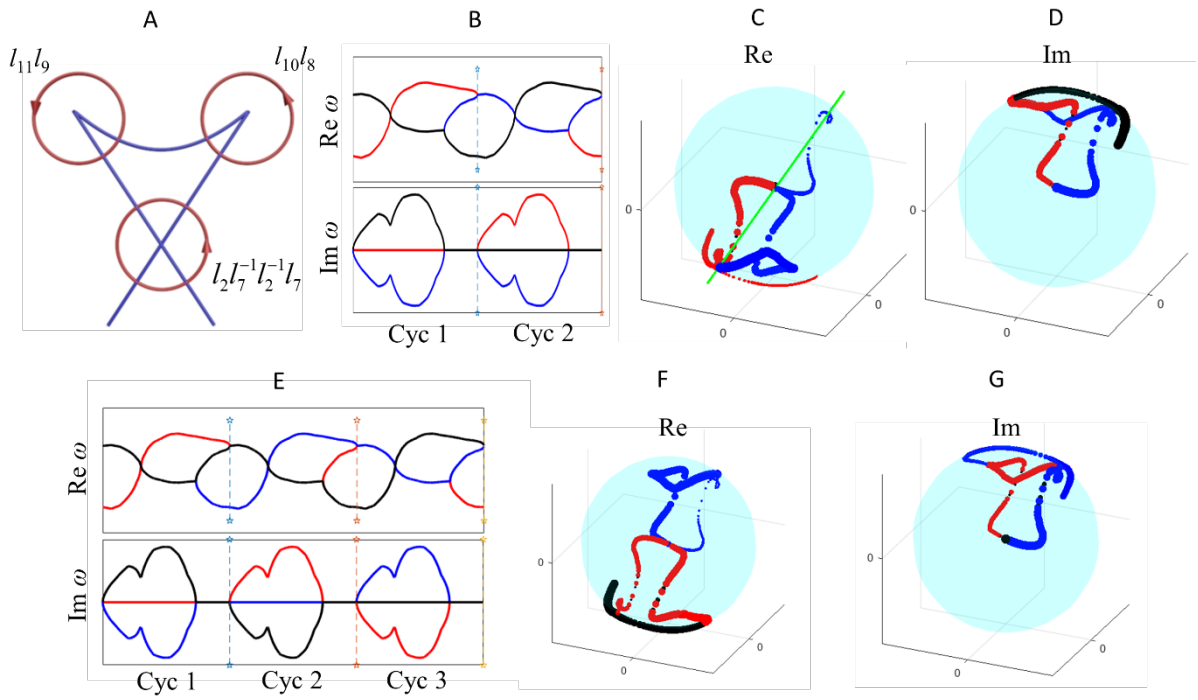

Fig. S5. Composite loops carrying hybrid topological invariant. A. Composite loops circulating EL3s (l_8l_{10} and l_9l_{11}) and NIL ($l_2l_7^{-1}l_2^{-1}l_7$). B and E. Evolution of eigenvalues on composite loop l_8l_{10} for invariants $\alpha_{10}\alpha_8^{-1}$ (for two cycles) and $\alpha_{10}\alpha_8^{-1}$ (for three cycles), respectively. (require discussions) C-D and F-G. Adiabatic transformation of eigenstates for invariants $\alpha_{10}\alpha_8^{-1}$ (for two cycles) and $\alpha_{10}\alpha_8^{-1}$ (for three cycles), respectively. C and F, real parts of eigenstates. D and G, imaginary parts of eigenstates.

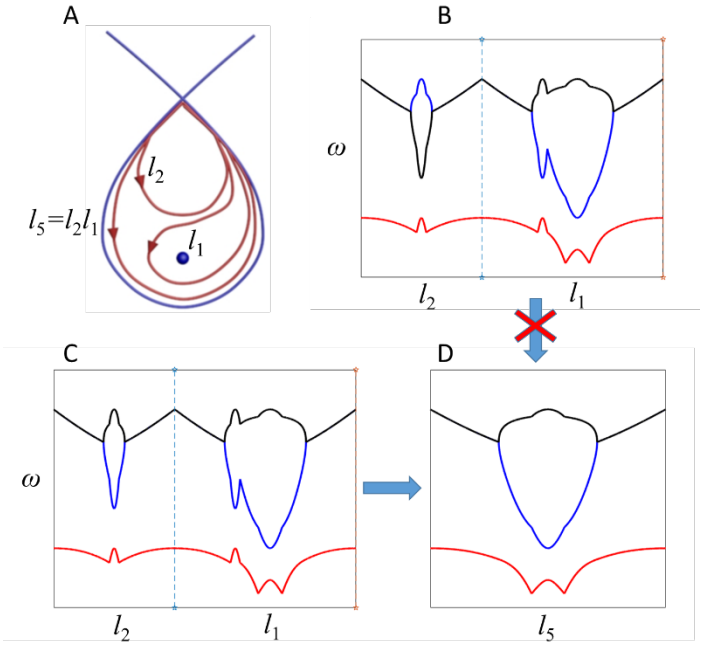

Fig. S6. Impact of the sequence of eigenvalues on opening basepoint. A. l_5 is the composite of l_1 and l_2. B. The common basepoint of l_1 and l_2 cannot be open if the sequences of eigenvalues (blue and black) are different on the two loops. On the contrary, the basepoint can be open if the sequence are identical on l_2 and l_1 (in C) and is equivalent to l_5 (in D).

The above analysis shows that it is important to specify the sequence of the two eigenstates (or eigenvalues) forming ES before discussing the topological invariant on a closed loop circulating a hypersurface singularity. Because different sequence of the two eigenstates will result in different invariant. For some composite loops, opening up the basepoint will set a constraint on the sequence of eigenstates. Let us take the loop l_5 (see Fig. S6) as an example. The loop l_5 is a composite of l_2 and l_1 in case that the sequence of eigenstates on l_2 is defined by the eigenvalues (from small to large). On the contrary, if we change the order of φ_2 and φ_3, l_5 has to be the composite of l_2 and l_{14} (see Fig. S6), and the basepoint cannot be open. This can be easily understood, because band 2 cannot continuously evolves to band 3 unless they coalesce (note that the basepoint is on NIL).

7. Other equivalent loops

In the maintext, we have shown some equivalent loops circulating degeneracy lines in the swallowtail, and explained the transition within different types of lines via the MT in view of the topological charge conservation. Here, we provide more equivalent loops as supplements, which also protects the emergence of the swallowtail.

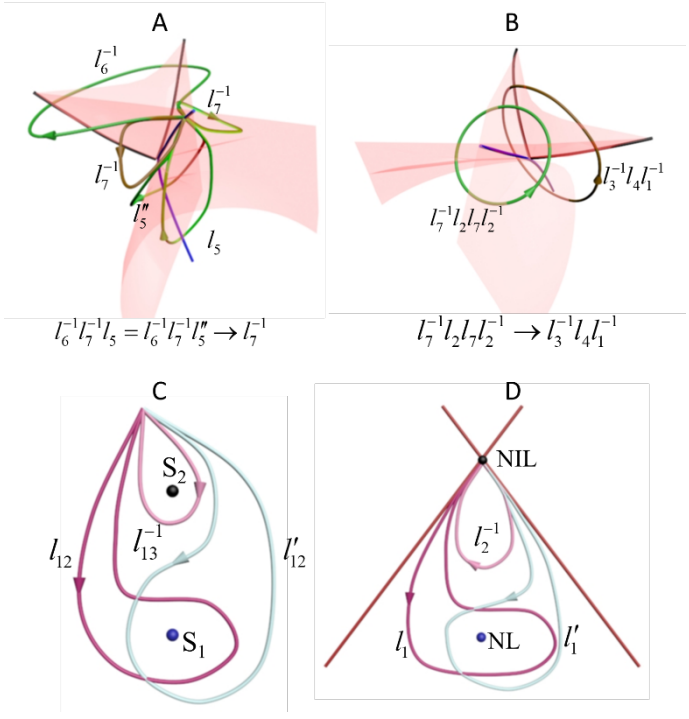

Fig. S7. Equivalent loops and commutation relations. A. The composite loop $l_6^{-1}l_7^{-1}l_5^{-1}$ is equivalent to l_7^{-1} and can be continuously deformed to each other. B. The NIL enclosed by $l_7^{-1}l_2l_7l_2^{-1}$ can transit to the double EL3s and NL circulated by $l_3^{-1}l_1^{-1}$ via the MT, due to topological charge conservation. C. Non-commutation relation of the topology of two isolated singularities. The inequality $l_{12}' \neq l_{12}$ holds because the singularity S_2 blocks the deformation process from l_{12} to l_{12}'. D. Commutation relation of the topology of an isolated singularity and a hypersurface singularity. The equality $l_1' = l_1$ holds because the NIL is on the loop l_2, which cannot prevent the deformation form l_1 to l_1'.

We have demonstrated that $l_7^{-1}l_5l_7 = l_6^{-1}$, and thus it can be easily derived that $l_7^{-1} = l_6^{-1}l_7^{-1}l_5^{-1}$. Since l_5, l_5' and l_5'' are equivalent, the basepoint of the composite $l_6^{-1}l_7^{-1}l_5^{-1}$ (shown in Fig. S7A) can be open, which is obviously equivalent to l_7^{-1}. Hence, the loop l_7^{-1} can be continuously deformed to $l_6^{-1}l_7^{-1}l_5^{-1}$, as shown in Fig. S7A. The deformation processes do not encounter other degeneracy lines, and thus the topological charge are conserved. Besides, a closed loop circulating the NIL can be continuously deformed to the loop circulating both the double EL3s and the NL (see Fig. S7B). The demonstration of the equivalence requires the commutation relations $l_2l_1 = l_1l_2$ and $l_7l_1 = l_1l_7$. This can be understood as the following. As shown in Fig. S7C, the loops l_{12} and l_{12}' circulate the singularity S_1 via different paths, and it is not difficult to discover that $l_{12}' = l_{13}^{-1}l_{12}l_{13}$, where the loop l_{13} encloses the singularity S_2. Generally the relation $l_{12}' = l_{12}$ does not hold [13,17], because l_{12}' cannot be continuously deformed to l_{12}, prevented by the isolated singularity S_2. However, the situation will be a little different if S_2 is a hypersurface singularity (see Fig. S7D). This is because the hypersurface singularity is on the loop, instead of being surrounded by a loop totally. Hence, it is not difficult to imagine that the loop l_1 can be continuously deformed to l_1', and no isolated singularity can prevent the deformation process (i.e. $l_2l_1 = l_1l_2$). Similarly, the other commutation relation $l_7l_1 = l_1l_7$ also holds. (require discussions) With the commutation relations, one can easily obtain $l_7^{-1}l_2l_7l_2^{-1} = l_3^{-1}l_1^{-1}$. The composite loop on the left hand side encloses the NIL, and since l_4 is trivial, the right hand side $l_3^{-1}l_1^{-1}$ is equivalent to $l_3^{-1}l_5l_1^{-1}$, which encloses the NL and the double EL3. Hence, $l_7^{-1}l_2l_7l_2^{-1}$ can be continuously deformed to $l_3^{-1}l_5l_1^{-1}$, and the double EL3 and the NL can transit to the NIL via the MT.

Reference

1. Helbig T, Hofmann T, Imhof S, et al. Generalized bulk–boundary correspondence in non-Hermitian topolectrical circuits[J]. Nature Physics, 2020, 16(7): 747-750.
2. Hofmann T, Helbig T, Lee C H, et al. Chiral voltage propagation and calibration in a topolectrical Chern circuit[J]. Physical review letters, 2019, 122(24): 247702.
3. Chen W K. The Circuits and Filters Handbook (Five Volume Slipcase Set)[M]. CRC Press, 2018.
4. Lu L. Topology on a breadboard[J]. Nature Physics, 2018, 14(9): 875-877.
5. Lee C H, Imhof S, Berger C, et al. Topolectrical circuits[J]. Communications Physics, 2018, 1(1): 1-9.
6. Imhof S, Berger C, Bayer F, et al. Topolectrical-circuit realization of topological corner modes[J]. Nature Physics, 2018, 14(9): 925-929.
7. Ningyuan, J., Owens, C., Sommer, A., Schuster, D. & Simon, J. Time-and siteresolved dynamics in a topological circuit. Phys. Rev. X 5, 021031(2015).
8. Helbig, T. et al. Band structure engineering and reconstruction in electric circuit networks. Phys. Rev. B 99, 161114 (2019).
9. Freedman D Z, Van Proeyen A. Supergravity[M]. Cambridge university press, 2012.

10. Schleich W P. Quantum optics in phase space[M]. John Wiley & Sons, 2011.

11. Shen H, Zhen B, Fu L. Topological band theory for non-Hermitian Hamiltonians[J]. Physical review letters, 2018, 120(14): 146402.

12. Young S M, Kane C L. Dirac semimetals in two dimensions[J]. Physical review letters, 2015, 115(12): 126803.

13. Wu Q S, Soluyanov A A, Bzdušek T. Non-Abelian band topology in noninteracting metals[J]. Science, 2019, 365(6459): 1273-1277.

14. Tang W, Jiang X, Ding K, et al. Exceptional nexus with a hybrid topological invariant[J]. Science, 2020, 370(6520): 1077-1080.

15. Main text

16. Arnol'd V I. Catastrophe theory[M]. Springer Science & Business Media, 2003

17. Mermin, N. David. "The topological theory of defects in ordered media." Reviews of Modern Physics 51.3 (1979): 591.